Modeling and Implementation of Active Magnetic Bearing Rotor System for FPGA-based Control

Rafał Jastrzębski, Riku Pöllänen and Olli Pyrhönen
Dept. of Electrical Engineering
LUT
P.O. Box 20, FIN-53851
Lappeenranta, Finland
rafal.jastrzebski@lut.fi

Antti Kärkkäinen
Dept. of Mechanical Engineering
LUT
P.O. Box 20, FIN-53851
Lappeenranta, Finland
antti.karkkainen@lut.fi

Jussi Sopanen
Faculty of Technology
South Carelia Polytechnic
Pohjolankatu 23, FIN-53101
Lappeenranta, Finland
jussi.sopanen@scp.fi

***Abstract* – This article reveals an implementation of a flexible rotor model with the nonlinear actuator for an LQ-control realization using field programmable gate arrays. The presented AMB-rotor model can be utilized both for the controller (as a state observer and nonlinearity compensator) and for the system development as a real-time plant emulator. The different variants of the LQ position control are considered in regard to the rotor model, used as a part of the observer. The model of the studied rotor was obtained using the finite element modeling, modal reduction technique and experimental analysis.**

***Index Terms* – Magnetic levitation, magnetic bearings, digital control, linear-quadratic control**

I. Introduction

A digital control of an active magnetic bearing system is a very demanding engineering task, when real-time embedded realization is considered. From the control point of view the active magnetic bearing (AMB) rotor system is unstable, nonlinear, multivariable plant with varying parameters and residual dynamics. When in fact, the most commonly employed control methods are simple linear ones, notably PID-based (e.g., a decentralized PID feedback as in [1]) and rotating rigid body model-based control methods, e.g. [2] and [3]. These techniques are feasible for many control applications. However, in the case of high speed rotating machines, highly flexible rotors and external disturbance forces, a high performance control is required. Therefore, influence of flexible rotor modes and actuator nonlinearities should be taken into account in the controller. In particular the physical limitations point at the formulation of the control strategy as a linear-quadratic (LQ) optimization problem. The LQ optimal control, as suggested in [4], seems to be a suitable control method for the AMB system. Compared to the above references, the presented LQ optimal control solution is applied to the flexible rotor and it differs in the usage of a full current state observer, disturbance observer and utilization of Bryson's rules [5].

Digital implementations of the control of electromechanical systems are typically based on digital signal processors (DSPs), but the realizations of pulse wide modulators and other actuators, which are based on field programmable gate arrays (FPGAs) are not uncommon. For the DSP-based realizations the major limiting factor is the computational burden of the high performance real-time feedback controller. FPGAs are more flexible and have greater advantage in handling many inputs and outputs, not to mention the possibilities of parallel computing. Nonetheless, the design and testing of FPGA implementations are usually more difficult and time consuming than in the case of DSPs. There are very few examples of the FPGA-based implementations of the magnetic levitation system controllers in the literature (e.g., [6], [7]). This article presents the FPGA-based realization of the AMB-rotor system, which can be used as the part of a single chip controller as well as a real-time plant emulator.

The AMB-rotor system is divided into two subsystems: a set of two radial bearings (axial suspension is considered separately), which act as actuators, and the flexible rotor model. Before the control synthesis and its implementation the appropriate models for these subsystems have to be formed.

II. Model of the AMB Actuators

An eight-pole radial bearing with a differential driving mode is assumed. The control of the attractive forces is performed with the control currents i_{cx}, i_{cy} while the pre-magnetization current i_0 (bias current) is applied to all coils.

A. Approximation of the force-current-characteristics

The force-current-position characteristics of the radial active magnetic bearings were studied using a two-dimensional reluctance network method [8], which took into account a magnetic saturation, cross coupling and leakage flux over the stator slots. The force versus current and position characteristics (for the reduced pre-magnetization current) obtained by the RNM is depicted in Fig. 1. For testing the controllers we introduced the attractive force non-linear relation as a look-up table and multivariable interpolation. Consequently, the rotor model used together with the force-field model has a force vector as an input. For the purpose of control synthesis the current and position dependent magnetic force, in the x-axis of one of the magnetic bearings, can be formed as

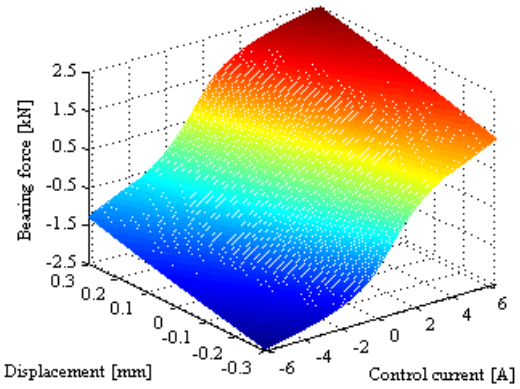

Fig. 1. Force versus current and position characteristics

$$F_{1x} = \frac{1}{4}\upsilon\mu_0 N^2 A \cos\zeta\left(\left(\frac{i_0 + i_{cx}}{x_0 - x}\right)^2 - \left(\frac{i_0 - i_{cx}}{x_0 + x}\right)^2\right) \quad (1)$$

where N, A, ζ, υ, μ_0, x and x_0 are the total number of coil turns in the electromagnet, area of the pole face, force acting angle, leakage factor, permeability of vacuum, position and air gap, respectively. Due to the differential driving mode the relation can be linearized in the vicinity of the operating point as

$$F_{1x}(x, i_{cx}) = k_i i_{cx} + k_x x \quad (2)$$

where k_i and k_x are the current stiffness and position stiffness, respectively.

B. *Approximation of the Actuator Dynamics*

The currents in the actuators are controlled by the internal, in regard to the external position control, current control loops. The proportional and feedforward controllers control the coils' currents. The fast current feedback compensates variations in the coil inductance. The feedforward gain compensates the effect of a resistive voltage drop and non-idealities in the gate drivers. For the simulation purposes the internal current control loop is modeled as a close-loop proportional and feedforward controlled LR-circuit with the modulation delay. The approximated transfer function, suitable for the position control synthesis, from the reference current i_c to the coil current i_m is expressed as

$$T(s) = G_P / (sL + R + G_P) \quad (3)$$

where G_P, L and R stand for the proportional controller gain, coil inductance and resistance, respectively.

III. Model of the Studied Rotor

Studied structure is a rotor with the stacks of steel laminations, which are for magnetic bearings, and couplings on the ends of the rotor. Aluminium sleeves and lock nuts are used to assemble the stack of steel laminations. Properties of all material are presented in Table I. Laminations' modulus of elasticity is assumed to be zero because in practice it does not carry any shearing stresses. Respectively, the modulus of elasticity of the aluminium sleeves is determined with the help of the experimental modal analysis that is discussed in the following section. The mass of the rotor is 54 kg and the length and largest diameter of the rotor are 1185 mm and 85 mm, respectively. The polar and diametral mass moments of inertia of the rotor are 0.06 kgm^2 and 7.24 kgm^2.

A. *Used Elements of the Rotor*

The rotor and the laminations under investigation are modeled using beam finite elements. The beam elements are based on the Timoshenko beam theory, which accounts for the shear deformation of the cross-section. Analysis of the rotor is concentrated on lateral vibration of the rotor and for this reason, axial and torsion degrees of freedom are neglected. In the modeling of the rotor the continuous elastic shaft is divided into discrete finite elements, which are connected at station points. The element with eight degree-of-freedom is assumed to be homogenous with distributed stiffness and mass. The cross-section of the shaft is assumed to be rigid. Therefore, the configuration of the element can be parameterized, by employing the centerline, as in [9].

The couplings on the ends of the rotor are modeled using rigid disc elements with four degree-of-freedom. In addition, the gyroscopic effect is included in the disc element.

B. *Equations of Motion*

Matrices that describe the complete rotor system can be formed using a standard assembly procedure of the finite element method. Equations of motion for rotor bearing system can be written as follows

$$\mathbf{M}\ddot{\mathbf{q}} + (\mathbf{C} + \Omega\mathbf{G})\dot{\mathbf{q}} + \mathbf{K}\mathbf{q} = \mathbf{F}(t) \quad (4)$$

where $\mathbf{M}$ is the mass matrix, $\mathbf{C}$ viscous damping matrix, $\mathbf{G}$ gyroscopic matrix and $\mathbf{K}$ the stiffness matrix. Vector $\mathbf{q}$ is a vector of system's degrees of freedom, $\mathbf{F}$ is a vector of externally applied forces and Ω is the angular velocity of the rotor.

A time integration schemes can be used for solving (4). However, equations are coupled and the system has many degrees of freedom. As a result, numerical solution is time consuming. The number of system's degrees of freedom can be reduced using modal coordinates instead of the nodal coordinates. This method will also lead to an uncoupled system of equations in case of symmetric positive definite matrices [10]. The normal modes are obtained by solving the following eigenvalue problem:

$$\left[\mathbf{K} - \omega_k^2 \mathbf{M}\right]\boldsymbol{\varphi}_k = \mathbf{0} \quad (5)$$

where ω_k^2 and $\boldsymbol{\varphi}_k$ are the kth eigenvalue and eigenvector.

TABLE I
Material Properties

Material	Modulus of elasticity (GPa)	Poisson's ratio	Shear modulus (GPa)
Steel	206.0	0.30	79.2
Aluminium	10.3	0.35	1.0
Lamination	0.0	0.30	1.0

As many modes as the system has degrees of freedom can be extracted. However, in practice, only few lowest frequency modes contribute significantly to the response of the system. Therefore, high frequency modes can be neglected without a significant loss of accuracy.

In the modal reduction technique, only few lowest frequency modes are retained. The matrix of the normal modes can be obtained using n_m number of eigenvectors, as follows:

$$\mathbf{\Phi} = \begin{bmatrix} \boldsymbol{\varphi}_1^N & \cdots & \boldsymbol{\varphi}_{n_m}^N \end{bmatrix}. \tag{6}$$

The coordinate transformation that relates the modal coordinates, $\mathbf{p}$, to the physical coordinates, $\mathbf{q}$, is:

$$\mathbf{q} = \mathbf{\Phi p}\ . \tag{7}$$

Equation (4) can now be written using modal coordinates as follows

$$\mathbf{M}_m\ddot{\mathbf{p}} + (\mathbf{C}_m + \Omega\mathbf{G}_m)\dot{\mathbf{p}} + \mathbf{K}_m\mathbf{p} = \mathbf{F}_m(t) \tag{8}$$

where subscript m indicates modal matrix.

Vector of modal coordinates, $\mathbf{p}$, can now be solved using a time integration. Physical displacements can be solved from (7) when the modal coordinates are known. The number of equations is equal to the number of retained modal coordinates. The original system of (4) can contain up to 200 degrees of freedom in case of realistic industrial rotor. This kind of system can be usually described with sufficient accuracy using only 4-10 modal coordinates.

IV. Modal Analysis of Studied Rotor

Modal analysis is a procedure of determining structure's dynamic characteristics, i.e. the natural frequencies, damping ratios, and mode shapes. The key to modal analysis are the relationship between the applied force and structure's responses. This relationship is computed as functions of frequency in terms of magnitude, phase and coherence. The required structural parameters are extracted from the measured frequency response functions by a process of curve fitting.

In the measurements the studied rotor is hoisted up with flexible rubber ropes. The accelerometer position is fixed and the hammering point is varied, which is called a roving hammer procedure. Direction of impacts is in horizontal direction. The measurement was performed for rotor with stacks of steel laminations and couplings. The objective of modal analysis was to compare the calculated natural frequencies and mode shapes to the measured ones.

The percentage differences between the measured and calculated frequencies and the modal damping ratios are presented in Table II. The differences between the measured and calculated modes are presented in Fig. 2, where a solid line indicates the calculated mode and dots indicate the measured points of that mode.

Overall the results between the measured frequencies and calculated ones are in line. Especially the first calculated frequency is accurate; the difference between frequencies is smaller than 0.1 %. Frequencies of higher modes are less accurate. However, the calculated modes are same as measured.

TABLE II
Measured and Calculated Free-free Frequencies of the Rotor

Mode #	Calculated frequency (Hz)	Measured frequency (Hz)	Difference (%)	Measured damping (%)
1	193.6	193.5	0.1	0.1635
2	402.6	397.0	1.4	0.0549
3	762.1	767.5	0.7	0.0641
4	1206.6	1238.0	2.6	0.1157

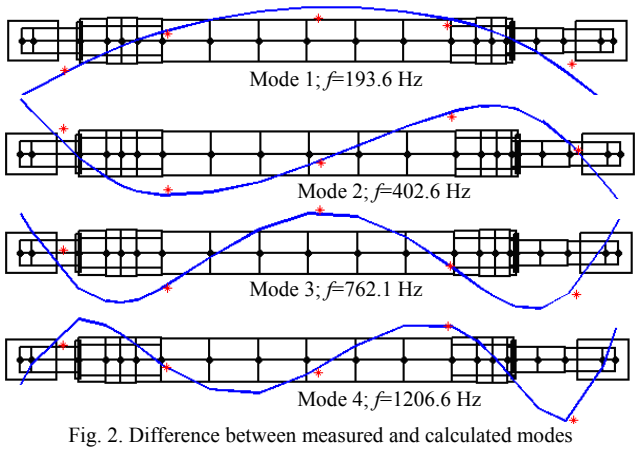

Fig. 2. Difference between measured and calculated modes

The modeled structure includes non-idealities, which affect the calculation. One non-ideality is friction between jointed components. The friction is difficult to define because the sleeves and the laminations are not tight fitted to the rotor. The most relevant non-idealities are stacks of steel laminations. Because of their structure, they are modeled without any bending stiffness at all.

V. LQ-Control and Non-Linearity Compensation

In this chapter the continuous-time models are considered for the sake of the clear presentation. Firstly, based on the equation of motion (8) the state-space model of the rotor is formed as in [11]. Then, adding the obtained rotor state-space model to the actuator and filter for the measured positions, we obtain an overall system model in a state-variable form

$$\dot{\mathbf{x}} = \mathbf{Ax} + \mathbf{Bu}\ ,\ \mathbf{y} = \mathbf{C}_s\mathbf{x} + \mathbf{Du}\ , \tag{9}$$

such as

$$\begin{bmatrix} \dot{\mathbf{x}}_a \\ \dot{\mathbf{x}}_r \\ \dot{\mathbf{x}}_f \end{bmatrix} = \begin{bmatrix} \mathbf{A}_a & \mathbf{0} & \mathbf{0} \\ \mathbf{B}_r\mathbf{C}_a & \mathbf{A}_r & \mathbf{0} \\ \mathbf{0} & \mathbf{B}_f\mathbf{C}_r & \mathbf{A}_f \end{bmatrix} \begin{bmatrix} \mathbf{x}_a \\ \mathbf{x}_r \\ \mathbf{x}_f \end{bmatrix} + \begin{bmatrix} \mathbf{B}_a \\ \mathbf{0} \\ \mathbf{0} \end{bmatrix} \mathbf{i}_c \tag{10}$$

$$\mathbf{x}_m = \begin{bmatrix} \mathbf{0} & \mathbf{0} & \mathbf{C}_f \end{bmatrix} \mathbf{x} \tag{11}$$

where the $\mathbf{x}_m$ represents the measured positions in the sensors' locations and $\mathbf{x}$, $\mathbf{u}$, $\mathbf{y}$, $\mathbf{i}_c$ are the vectors of state variables, input variables, outputs and control currents, respectively. The subscripts a, r and f denote relation to the actuator, rotor and filter, respectively.

A. Designing the LQ position control

At first, the feedback gains $\mathbf{K}_s$ and the additional integral feedback gains $\mathbf{K}_I$ are computed such that the

state-feedback law minimizes the quadratic integral performance index

$$J = \int_0^\infty \left[\mathbf{x}^T \mathbf{Q}_1 \mathbf{x} + \mathbf{u}^T \mathbf{Q}_2 \mathbf{u}\right] dt \tag{12}$$

where the weighting matrices $\mathbf{Q_1}$ and $\mathbf{Q_2}$ are based on the physical constraints, i.e., using a guideline, sometimes called Bryson's rules [5]. Secondly, the optimal in the least-square sense predictor estimator gain matrix $\mathbf{L_p}$ and the disturbance estimator gain matrix $\mathbf{L_w}$ are computed. The computation is based on the covariance matrices formed from the rms accuracy of the position measurements and control inputs. Eventually, the obtained state-space controller can be presented in normal state-variable form, where the disturbance estimate vector $\overline{\mathbf{w}}$ enters the system through the state estimator inputs (not through the control inputs) and the current estimated state vector $\hat{\mathbf{x}}$ is based on the current position measurements $\mathbf{x_m}$. Accordingly, let us assemble the state-space observer, such as

$$\dot{\mathbf{x}}_{ob} = \begin{bmatrix} \mathbf{0} & \mathbf{0} & \mathbf{0} \\ \mathbf{0} & \mathbf{A} - \mathbf{L_p C_s} & \mathbf{B} \\ \mathbf{0} & -\mathbf{L_w C_s} & \mathbf{A_w} \end{bmatrix} \mathbf{x}_{ob} + \begin{bmatrix} \mathbf{K_i} & \mathbf{0} & -\mathbf{K_i} \\ \mathbf{0} & \mathbf{B} & \mathbf{L_p} \\ \mathbf{0} & \mathbf{0} & \mathbf{L_w} \end{bmatrix} \mathbf{u}_{ob} \tag{13}$$

$$\mathbf{y}_{ob} = \begin{bmatrix} \mathbf{I} & \mathbf{0} & \mathbf{0} \\ \mathbf{0} & -\mathbf{L_c C_s} + \mathbf{I} & \mathbf{0} \\ \mathbf{0} & \mathbf{0} & \mathbf{0} \end{bmatrix} \mathbf{x}_{ob} + \begin{bmatrix} \mathbf{0} & \mathbf{0} & \mathbf{0} \\ \mathbf{0} & \mathbf{0} & \mathbf{L_c} \\ \mathbf{0} & \mathbf{0} & \mathbf{0} \end{bmatrix} \mathbf{u}_{ob} \tag{14}$$

$$\mathbf{x}_{ob} = \left[\mathbf{x_i} \quad \overline{\mathbf{x}} \quad \overline{\mathbf{w}}\right], \quad \mathbf{y}_{ob} = \left[\mathbf{x_i} \quad \hat{\mathbf{x}} \quad \overline{\mathbf{w}}\right] \tag{15}$$

$$\mathbf{u}_{ob} = \left[\mathbf{x_{ref}} \quad \mathbf{i_c} \quad \mathbf{x_m}\right], \quad \mathbf{L_c} = \mathbf{A}^{-1}\mathbf{L_p} \tag{16}$$

where $\mathbf{x_i}$, $\overline{\mathbf{x}}$, $\mathbf{x_{ref}}$ describe the vectors of the integral state variables, predictor estimated state variables and reference positions, respectively. Then, we consider two variants of the regulator

$$\mathbf{i_c} = \mathbf{C_{reg}} \mathbf{y}_{ob} + \mathbf{D_{reg}} \mathbf{u}_{ob} \,. \tag{17}$$

The first variant is

$$\mathbf{C_{reg1}} = \left[\mathbf{I} \quad -\mathbf{K_s} \quad \mathbf{0}\right], \quad \mathbf{D_{reg1}} = \left[\mathbf{0} \quad \mathbf{0} \quad \mathbf{0}\right] \tag{18}$$

and the second one is

$$\begin{aligned} \mathbf{C_{reg2}} &= \left[\mathbf{I} \quad \left[-\mathbf{K_a}, \mathbf{0}, \mathbf{K_{rig}} \mathbf{C_{rig}}^{-1} \mathbf{C_{oth}} - \mathbf{K_o}, -\mathbf{K_f}\right] \quad \mathbf{0}\right] \\ \mathbf{D_{reg2}} &= \left[\mathbf{0} \quad \mathbf{0} \quad -\mathbf{K_{rig}} \mathbf{C_{rig}}^{-1}\right] \end{aligned} \tag{19}$$

where the rotor output matrix $\mathbf{C_r}$ is split into two parts [$\mathbf{C_{rig}}$, $\mathbf{C_{oth}}$] corresponding to the rigid body modes and to the remaining rotor state variables, respectively. The feedback gain matrix $\mathbf{K_s}$ is split into four parts [$\mathbf{K_a}$, $\mathbf{K_{rig}}$, $\mathbf{K_o}$, $\mathbf{K_f}$] corresponding to the actuator, rigid rotor modes, other rotor state variables and filter, respectively.

B. Designing the non-linearity compensation

We utilized the inverse nonlinearity control method in order to compensate the nonlinearities in the AMB actuator. The method assumes that nonlinearity is invertible and can be undone. The compensation principle is presented in Fig. 3. The usage of this method for AMBs was studied in [12], where the analytical methods were employed, and in [13], [14], where a polynomial formulation was used. In order to compensate actuator nonlinearities we introduce the attractive force non-linear relation (into the AMB controller) as a look-up table and multivariable interpolation. The inverted relation (depicted in Fig. 4) of the aforementioned force-current characteristics was determined by the means of high polynomials fitting and stored in the appropriate table. One has to bear in mind, that when the compensation of the actuator is incorporated into the controller as the nonlinearity inverse approximation, the control input becomes force F_r instead of current i_c, whereas the position stiffness k_x and current stiffness k_i are canceled out from the close-loop system dynamics (i.e., the position control has to be redesigned accordingly).

VI. FPGA-BASED IMPLEMENTATION

For a discrete-time implementation a discrete equivalents of (9), at sampling period T_s, can be obtained by using a zero-order-hold (ZOH). However, before that in regard to a fixed-point number representation in the FPGA, proper per-unit values have to be derived. A per-unit (pu) system is the dimensionless relative value system defined in the terms of base values. The fundamental base values are selected as equal to maximum attainable physical values (e.g., maximum current, air gap length, etc). The per-unit scaling is based on the physical quantities, the eigenvectors in the flexible rotor model are scaled so that the maximum deformation of each bending mode equals 1 (m). Finally, the general continuous-time state-space model (9), can be transformed as

$$\begin{aligned} \dot{\mathbf{x}}^{\mathbf{pu}} &= \mathbf{T A T}^{-1} \mathbf{x}^{\mathbf{pu}} + \mathbf{T B T_u}^{-1} \mathbf{u}^{\mathbf{pu}} \\ \mathbf{y}^{\mathbf{pu}} &= \mathbf{T_y C_s T}^{-1} \mathbf{x}^{\mathbf{pu}} + \mathbf{T_y D T_u}^{-1} \mathbf{u}^{\mathbf{pu}} \end{aligned} \tag{20}$$

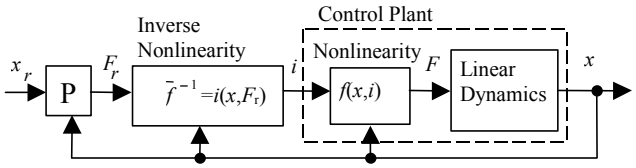

Fig. 3. The compensation principles of the nonlinear actuator using the approximate inverse nonlinearity, where **P**, x_r, F_r are position control, position reference and force reference, respectively.

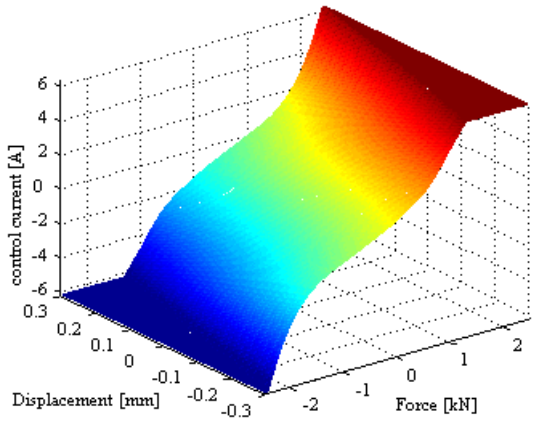

Fig. 4. Inverted relation of force-current-position characteristics

where $\mathbf{T}$, $\mathbf{T_u}$, $\mathbf{T_y}$, are the diagonal state transformation matrices. The transformation matrices have their diagonal entries based on the fundamental base values.

The AMB actuator and the rotor model are implemented in the Xilinx's Virtex2Pro FPGA circuit using a hardware description language VHDL. The operational frequency is 100MHz.

A. *Force-field Interpolation*

Two alternative implementations of the non-linear force relation are presented. The solutions are based on a spatial interpolation and look-up table algorithms. The algorithms are described as for the inverse nonlinearity interpolation.

The first one is based on the original but sparser current matrix. After breaking the displacement and force into scaled integer and fractional parts x_{frac}, y_{frac}, the four closest entry current values are obtained and multiplied by the appropriate opposite square areas A (e.g., $A_{11}=x_{frac}y_{frac}$, $A_{22}= x_{frac}(1-y_{frac})$). The interpolated current value is the sum of the aforementioned multiplications.

The second method is based on the piece-wise interpolation with second order surface. The piecewise surface coefficients are calculated by multiple regression method and stored in the look-up table. The result is obtained directly from the surface equation. The implementations details of the two methods are compared in Table III.

B. *Arithmetic Unit for the State-variable Form*

The most straightforward implementation of the controller or plant equations in the state-variable form seems to be the one, which utilizes the commercial ready-made embedded processors (e.g. the Xilinx's MicroBlaze or PowerPC). However, the custom arithmetic unit has the advantage over the general ones, with regard to the balancing utilized resources, computational power and number format accuracy.

For the presented LQ-control of the flexible rotor, when using the ZOH discrete equivalent with T_s=50μs and including the 8 flexible modes (4 modes in *xz*- and 4 modes in *yz*-plane) in the state observer, a simple pipelined multiply-accumulate (MAC), used as the arithmetic unit is sufficient. The implementation details of the simple arithmetic unit for state-variable models are given in Table IV. As an example the plant model with 12 flexible modes in the rotor is considered. In the model only the coefficients not equal to zero take part in the computation. In addition, for those applications where more complex models and faster sampling rates are required, few MAC units can be assembled to work in parallel. Furthermore, the usage of the double port block RAMs enables the parameters update by some slower external IP core, e.g. embedded processor.

VII. Testing the Controllers

The proposed LQ controllers, which feature rigid and flexible rotor models as a part of the observer, are tested in the simulations.

TABLE III
FPGA IMPLEMENTATION DETAILS OF FORCE-FIELD

Interpolation method	1). Sum of Areas	2). 2nd order surfaces
rms / maximum implementation error	0.71 / 4.12 N	0.72 / 8.88 N
(breakpoints) × coefficients	(30×50)×1	(30×30)×5
latency time of 1 / 5 interpolations	9 / 17 clock cycles	10 / 50 clock cycles
slices / hardware multipliers / BRAMs	212 / 4 / 2	151 / 1 / 8

TABLE IV
IMPLEMENTATION DETAILS OF STATE-VARIABLE FORM - PLANT

Flexible rotor model	12 flexible modes
latency time of one cycle - ZOH	1007 clock cycles
number format - variables / model coefficients / fraction	24-bit / 28-bit / 22-bit
slices / hardware multipliers / BRAMs	1078 / 4 / 6

Two tests are performed. At first, the step input reference position (equal to 0.6 pu) to the *x*-axis direction, at sensor one (at the 4th node in Fig. 2) is applied. Secondly, the artificial step disturbance force is applied through the bearing located at the 5th node in Fig. 2). The measured position responses in the x-axis direction, at the sensor one and 1-4 modal weighting factors are examined. All controllers are tested with the plant model, which features 12 flexible modes in the presence of the measurement noise and process noise.

The first tested controller includes only the rigid body modes in the observer, the regulator (18) and the fourth order sensor pre-filter, which eliminates a spillover from the residual modes as discussed in [15]. Its response is presented in Fig. 5. The applied disturbance force is equal to 40% of the force applied when testing the other controller.

The second controller features the flexible rotor with 8 flexible modes, the regulator (19) and the first order anti-aliasing filter. The applied disturbance force equals to 0.6 pu (1 pu equals the maximum achievable electromagnetic force in the direction of the electromagnet at the rotor central position with maximum current). The responses of two versions of this controller are presented in Fig. 6. Initially, the balanced weighting matrices $\mathbf{Q_1}$ and $\mathbf{Q_2}$ are used to slightly increase the damping of the flexible modes. Secondly, the scaling of the weighting matrices is such that the flexible modes are attenuated in expense of the rigid body modes. The active control of the flexible

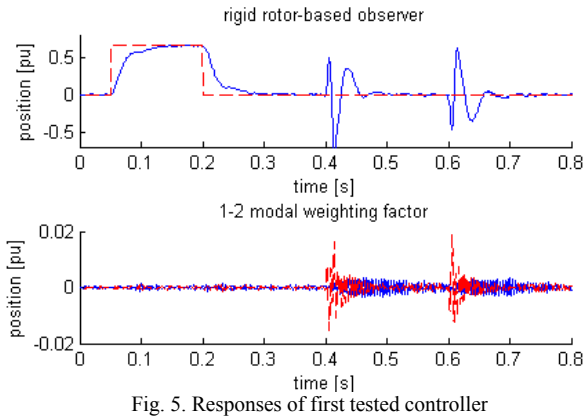

Fig. 5. Responses of first tested controller

modes (their attenuation) can be improved significantly, when accurate dynamic model of the close-loop current actuator is used in the observer. Finally, the non-linearity compensation is added to the second controller. The comparison between the responses of the compensated and non-compensated close-loop control systems (the applied disturbance force equals 0.66 pu) is depicted in Fig. 7.

The VHDL realization of the second controller and the plant emulator were validated using ModelSim simulator. The agreement with the corresponding Matlab simulations was found to be very good.

VIII. Conclusions

As long as the optimal control of the studied system is considered, the inclusion of the flexible rotor model in the control design provides advantages over the rigid rotor model-based control (faster control therefore bigger disturbance forces can be tolerated, active control of the flexible modes). However, such a control requires accurate plant model, faster sampling rates and more costly control

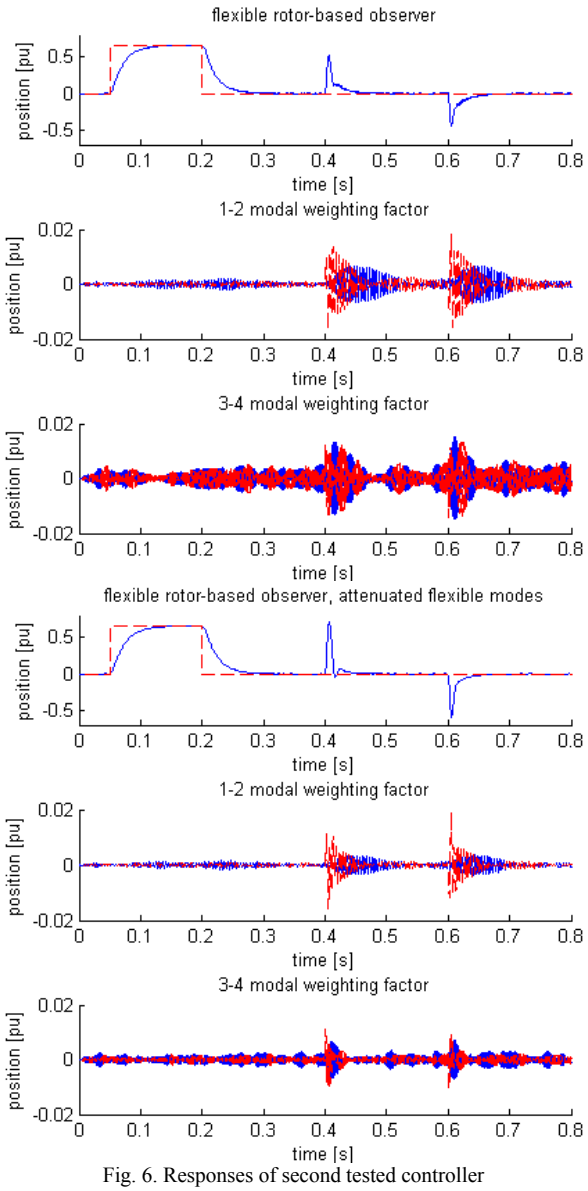

Fig. 6. Responses of second tested controller

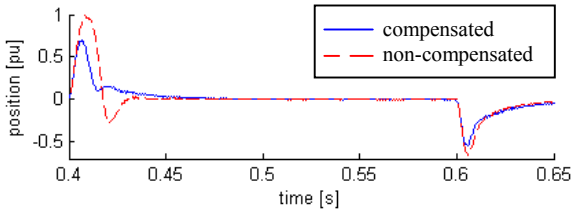

Fig. 7. Comparison of compensated and non-compensated control

electronics, e.g. fast ADCs and increased computational burden. Moreover, the more complex rotor model is used in the observer, the more parameters vary with Ω, and therefore the control system is more difficult to update.

The use of the FPGA alleviates a computationally heavy burden of the flexible rotor real-time implementation. Owing to the accurate modeling of the actuator also the bearing nonlinearities can be incorporated into the FPGA-based controller. Last but not least, FPGAs deliver a flexibility and parallelism to implementation of demanding control schemes and therefore they are attractive for realization of the high performance AMB-rotor control systems.

References

[1] B. Polajzer, J. Ritonja, G. Stumberger, D. Dolinar, J.-P. Lecointe, "Decentralized PI/PD position control for active magnetic bearings", *Electrical Engineering*, [Online], 2005. Available: http://www.springerlink.com.

[2] Schweitzer, G., Bleuler, H. and Traxler, A., 2003, *Active Magnetic Bearings*, Authors Reprint, Zurich.

[3] Wurmsdobler, P., 1997, *State Space Adaptive Control for a Rigid Rotor Suspended in Active Magnetic Bearings*, Ph.D. Dissertation, Vienna University of Technology, Vienna.

[4] Y. N. Zhuravlyov, "On LQ-Control of Magnetic Bearing", IEEE Trans. on Control Systems Technology, Vol. 8, No. 2, pp. 344-350, 2000.

[5] Franklin, G. F., Powell, J. D. and M. Workman, M., 1998, *Digital Control of Dynamic Systems*, 3rd ed. Addison Wesley.

[6] C. Oberbeck, H. Ulbrich, "Investigations in a Software-based Design of Linear Electromagnetic Actuators", *Proc. 8th Int. Symposium on Magnetic Bearings*, Mito, Japan, pp. 157-162, 2002.

[7] K.-J. Hoffmann, D. Laier, R. Markert, F.-M. Renner, M. Glesner, "Integrated Active Magnetic Bearings". *Proc. 6th Int. Symposium on Magnetic Bearings*, Edited by P. E. Allaire, Technomic Publ. Lancaster/Basel, pp. 256-265, 1998.

[8] J. Nerg, R. Pöllänen, O. Pyrhönen, "Modelling the Force versus Current Characteristics, Linearized Parameters and Dynamic Inductance of Radial Active Magnetic Bearings Using Different Numerical Calculation Methods", *WSEAS Trans. on Circuits and Systems*, Issue 6, Vol. 4, pp. 551-559, 2005.

[9] Chen, W. J. and Gunter, E. J., 2005, *Introduction to Dynamics of Rotor-Bearing Systems*, Trafford Publishing, Victoria, Canada.

[10] Genta, G., 2005, *Dynamics of Rotating Systems*, Springer, New York, USA.

[11] G. Genta, C. Delprete, S. Carabelli, "Active Magnetic Bearing Control Loop Modeling for a Finite Element Rotordynamics Code", *II Int. Symp. on Magnetic Suspension Technology*, Seattle, Agosto, pp. 319-333, 1993.

[12] N. Skricka, R. Markert, "Improvements in the Integration of Active Magnetic Bearings", *Proc. Control Engineering Practice*, vol. 10, Issue 8, pp. 917-922, 2002.

[13] J. E. Bonilla, V. H. Grisales, M. A. Melgarejo, "Genetic tuned FPGA based PD fuzzy LUT controller", *IEEE Proc. of the Int. Conf. on Fuzzy Systems*, Vol. 3, pp. 1084 -1087, 2001.

[14] F. Krach, B. Frackelton, J. Carletta, R. Veillette, "FPGA-Based Implementation of Digital Control for a Magnetic Bearing", *IEEE Proc. of the American Control Conf.*, Vol. 2, pp. 1080-1085, 2003.

[15] M. J. Balas, "Feedback Control of Flexible Systems", *IEEE Trans. on Automatic Control*, vol. 23, Issue 4, pp. 673-679, 1978.